Coupled Inertial Navigation and Flush Air Data Sensing Algorithm for Atmosphere Estimation

Christopher D. Karlgaard*, Prasad Kutty†
Analytical Mechanics Associates, Inc., Hampton, VA

Mark Schoenenberger‡
NASA Langley Research Center, Hampton, VA

This paper describes an algorithm for atmospheric state estimation that is based on a coupling between inertial navigation and flush air data sensing pressure measurements. In this approach, the full navigation state is used in the atmospheric estimation algorithm along with the pressure measurements and a model of the surface pressure distribution to directly estimate atmospheric winds and density using a nonlinear weighted least-squares algorithm. The approach uses a high-fidelity model of atmosphere stored in table-look-up form, along with simplified models of that are propagated along the trajectory within the algorithm to provide prior estimates and covariances to aid the air data state solution. Thus, the method is essentially a reduced-order Kalman filter in which the inertial states are taken from the navigation solution and atmospheric states are estimated in the filter. The algorithm is applied to data from the Mars Science Laboratory entry, descent, and landing from August 2012. Reasonable estimates of the atmosphere and winds are produced by the algorithm. The observability of winds along the trajectory are examined using an index based on the discrete-time observability Gramian and the pressure measurement sensitivity matrix. The results indicate that bank reversals are responsible for adding information content to the system. The algorithm is then applied to the design of the pressure measurement system for the Mars 2020 mission. The pressure port layout is optimized to maximize the observability of atmospheric states along the trajectory. Linear covariance analysis is performed to assess estimator performance for a given pressure measurement uncertainty. The results indicate that the new tightly-coupled estimator can produce enhanced estimates of atmospheric states when compared with existing algorithms.

Nomenclature

$\boldsymbol{C}$	=	Backward smoothing gain
$\boldsymbol{F}$	=	Linearization of $\boldsymbol{f}$ with respect to $\boldsymbol{x}$
$\boldsymbol{f}$	=	Low-fidelity atmospheric model equations of motion
$\boldsymbol{G}$	=	Linearization of $\boldsymbol{f}$ with respect to $\boldsymbol{u}$
g	=	Gravitational acceleration, m/s^2
$\boldsymbol{H}$	=	Linearization of $\boldsymbol{h}$ with respect to $\boldsymbol{x}$
$\boldsymbol{h}$	=	Pressure distribution model, Pa
$\boldsymbol{I}$	=	Identity matrix
$\boldsymbol{J}$	=	Linearization of $\boldsymbol{h}$ with respect to $\boldsymbol{u}$
k	=	Integer time index
N	=	Integer time index of final pressure measurement
$\boldsymbol{P}$	=	Covariance of $\boldsymbol{x}$ after the measurement model update

*Supervising Engineer, Senior Member AIAA.
†Project Engineer.
‡Aerospace Engineer, Atmospheric Flight and Entry Systems Branch, Senior Member AIAA.

p_s	=	Static pressure, Pa
$\boldsymbol{p}$	=	Pressure measurement vector, Pa
$\boldsymbol{Q}$	=	Process noise spectral density
$\tilde{\boldsymbol{Q}}$	=	Process noise covariance
$\boldsymbol{R}$	=	Pressure measurement covariance matrix
$\tilde{\boldsymbol{R}}$	=	Pressure measurement covariance matrix augmented with navigation uncertainty
R	=	Planetary radius, m
$\Re$	=	Specific gas constant, J/kg-K
$\boldsymbol{S}$	=	Prior covariance of $\boldsymbol{x}$ from low fidelity model
$\boldsymbol{T}$	=	Prior covariance of $\boldsymbol{x}$ from high fidelity model
T	=	Atmospheric temperature, K
$\boldsymbol{u}$	=	Vehicle inertial state
v_n, v_e, v_d	=	Vehicle planet-relative north, east, and down velocity components, m/s
$\boldsymbol{W}_o$	=	Discrete-time observability Gramian
w_n, w_e, w_d	=	North, east, and down wind velocity components, m/s
$\boldsymbol{X}_{11}$, $\boldsymbol{X}_{12}$, $\boldsymbol{X}_{22}$	=	Van Loan integral sub-matrices
$\boldsymbol{x}$	=	Atmospheric state vector
$\boldsymbol{\epsilon}$	=	Pressure measurement error vector, Pa
θ, ϕ, ψ	=	Vehicle pitch, roll, and yaw attitude angles, rad
μ	=	Gravitational parameter, m^3/s^2
ρ	=	Density, kg/m^3
σ_{min}	=	Minimum singular value of the observability Gramian
$\boldsymbol{\Phi}$	=	State transition matrix
$\boldsymbol{\Omega}$	=	Covariance of $\boldsymbol{u}$

I. Introduction

The traditional approach for estimating freestream atmospheric conditions from Flush Air Data Sensing (FADS) systems is based on a multi-tiered approach in which first the air data state (typically dynamic pressure, Mach number, angle of attack, and angle of sideslip) is estimated from the measured pressures, and then secondly are combined with an Inertial Navigation System (INS) to estimate the freestream atmospheric conditions (density and winds). One example is from the Space Shuttle, in which air data from both FADS[1] deployable boom were combined with INS to produce estimates of winds.[2] In this approach, the differences between the INS-derived flow angles (planet-relative) and the air data-derived flow angles (wind-relative) are attributed to winds, which results in a system of nonlinear algebraic equations. By neglecting the vertical wind component, the problem reduces to two equations (angle of attack and sideslip differences) and two unknowns (north and east wind components), which can be solved numerically using a Newton-Raphson method. The method has several advantages in that it is simple and yields a direct estimate of winds from in-situ measurements based on the combination of inertial velocity and attitude and wind-relative flow angles. Limitations of the approach are that the method is singular for flight path angles of zero, and all instrumentation errors are mapped into the wind estimates rather being accounted for using an uncertainty model.

Several approaches for tighter coupling between FADS and INS have been proposed. One common technique is the use of complimentary filters[3,4] in which the attitude rates from INS are used to smooth the FADS attitude estimate. The complimentary filtering approach does not directly impact any estimates of the atmospheric conditions along the trajectory. Kalman filtering approaches have been proposed for wind and atmosphere estimation from INS and air data sensors in Refs. 5,8–14. Kasich and Cheng[5] developed an INS/FADS blended state estimator for computing freestream static pressure, but the wind components were not estimated. Conversely, Refs. 6–10 developed Kalman filtering approaches suitable for real-time implementation, but focus solely on estimating the atmospheric winds and do not address estimating the thermodynamic state of the atmosphere. Ref. 11 developed an algorithm for estimating longitudinal winds for improved flight control. Refs. 12–14 proposed full state Kalman filters for estimating freestream winds, pressure, and density, but were designed for post-flight data processing rather than for real-time applications.

In Ref. 14, a novel INS-aided FADS state estimation algorithm was developed in which the INS velocity magnitude was used in conjunction with estimates of static pressure and density to compute a Mach number pseudo-

measurement. This approach provided enhanced FADS state estimates for flight conditions in the hypersonic regime, where estimating Mach number from pressures alone is numerically problematic. The algorithm does not directly estimate freestream winds from the pressure measurement data, instead wind components are estimated using the approach proposed in Ref. 2.

In this paper, the concept of the INS-aiding approach for the FADS state estimation algorithm is extended to include attitude information in addition to velocity. This approach enables the estimation of winds directly from the FADS pressure measurements, by reformulating the state to include winds, density, and pressure. A reduced-order iterative Kalman filter method is implemented to blend information about the atmospheric state from the pressure measurements with prior knowledge of the atmosphere from models. These models can include tabulated high-fidelity models and simplified models for propagating the atmospheric state forward in time from one pressure measurement to the next. The algorithm is simple enough that real-time data processing is a possibility. A backward smoothing algorithm can also be utilized in post-flight data processing scenarios to provide improved estimates over the entire trajectory.

The remainder of this paper is organized as follows. Section II describes the proposed atmospheric state estimator, including models and the filter/smoother algorithms. Section III applies this algorithm to the processing of FADS data from the recent Mars Science Laboratory mission, and compares results with previously published data from Ref. 14. Section IV describes how this algorithm can be used to benefit the Mars 2020 mission, including optimization of pressure port layout and transducer requirements development. Concluding remarks are given in Section V. Note that the main interest in this paper is for entry vehicle air data processing, however, the algorithm is general enough that it could be used for wider applications such as high speed aircraft.

II. Atmospheric State Estimation

The new approach for FADS state estimation proposed in this paper is to use the full state from the on-board navigation system (velocity and attitude) combined with the pressure data to directly estimate the atmospheric conditions. The estimation algorithm is aided by both high-fidelity atmospheric models tabulated vs. altitude and simplified atmospheric models that are propagated along the trajectory within the algorithm.

A. Pressure Modeling

The processing of pressure measurement data to produce estimates of the freestream atmospheric conditions requires a mathematical model of the pressures at each port location as a function of the atmospheric conditions. This pressure model can be based on one of several different approaches, such as modified Newtonian flow,[1] potential flow theory,[15] or tabulated CFD solutions.[14] In each case these models can include correction factors that are used to match the pressure models to wind tunnel test data. The pressure models are typically written as a function of angle of attack, angle of sideslip, Mach number, and dynamic pressure (or static pressure). In this paper, a new approach is taken and the form of the pressure model is recast to be a function of the inertial state of the vehicle (velocity and attitude), and the freestream atmospheric conditions (static pressure, density, and winds). Explicitly, the assumed model is of the form

$$\boldsymbol{p}_k = \boldsymbol{h}\left(\boldsymbol{x}_k, \boldsymbol{u}_k\right) + \boldsymbol{\epsilon}_k \tag{1}$$

where $\boldsymbol{p}_k$ are the pressures at each FADS port at time k, $\boldsymbol{x}_k = [\rho, p_s, w_n, w_e, w_d]^\intercal$ is the freestream atmospheric state, $\boldsymbol{u}_k = [v_n, v_e, v_d, \phi, \theta, \psi]^\intercal$ is the vehicle velocity and attitude state, and $\boldsymbol{\epsilon}_k$ is the combined pressure transducer measurement error and pressure model error, which is assumed to be zero mean with covariance $\boldsymbol{R}_k$.

B. Low-Fidelity Atmosphere Models

A low-fidelity model of the change in atmospheric conditions along the trajectory can be derived from basic idealized relations such as the hydrostatic equation and the perfect gas law. Such simplified relationships are suitable for implementation in the algorithm for propagating the atmospheric state estimate forward between pressure measurements, which are assumed to occur at a reasonably high rate (several samples per second) along the trajectory. Since the simplified model involves idealized approximations, uncertainties in the model can be accounted for with process noise.

A model for the rate of change in static pressure can be found by rewriting the hydrostatic equation as the time derivative of pressure along a given trajectory, namely

$$\dot{p}_s = \rho g v_d \tag{2}$$

Similarly, a model for the rate of change in density along the trajectory can be derived from the perfect gas law, with the assumption that the atmosphere is locally isothermal ($\dot{T} \approx 0$) between FADS pressure samples. The equation is of the form

$$\dot{\rho} = \frac{\dot{p}_s}{\Re T} = \frac{\dot{p}_s \rho}{p_s} = \frac{g v_d \rho^2}{p_s} \tag{3}$$

A reasonable simplified model for the rate of change in atmospheric winds is to assume a random walk model where the deterministic portion of the model is simply $\dot{w}_n = \dot{w}_e = \dot{w}_d = 0$. Thus, the low fidelity model can be written in the form

$$\dot{\boldsymbol{x}} = \boldsymbol{f}(\boldsymbol{x}, \boldsymbol{u}) + \boldsymbol{\eta} \tag{4}$$

where $\boldsymbol{\eta}$ is a process uncertainty term that is assumed to be zero mean with spectral density $\boldsymbol{Q}$, and

$$\boldsymbol{f}(\boldsymbol{x}, \boldsymbol{u}) = \left\{ \begin{array}{c} g v_d \rho^2 / p_s \\ \rho g v_d \\ 0 \\ 0 \\ 0 \end{array} \right\} \tag{5}$$

The continuous model in Eq. (4) can be transformed to a discrete model of the form,

$$\boldsymbol{x}_{k+1} = \boldsymbol{x}_k + \boldsymbol{f}(\boldsymbol{x}_k, \boldsymbol{u}_k) \Delta t \tag{6}$$

which is suitable for propagation between pressure measurements. The uncertainties in the model can be propagated between pressure measurements using the relation

$$\boldsymbol{S}_{k+1} = \boldsymbol{\Phi}_k \boldsymbol{S}_k \boldsymbol{\Phi}_k^\intercal + \boldsymbol{G}_k \boldsymbol{\Omega}_k \boldsymbol{G}_k^\intercal + \tilde{\boldsymbol{Q}}_k \tag{7}$$

where $\boldsymbol{\Phi}_k$ is the state transition matrix and $\tilde{\boldsymbol{Q}}_k$ is the discrete-time process noise covariance. These quantities can be jointly calculated from the Van Loan matrix integral,[17] given by

$$\exp\left(\left[\begin{array}{cc} -\boldsymbol{F}_k & \boldsymbol{Q}_k \\ \boldsymbol{0} & \boldsymbol{F}_k \end{array} \right] \Delta t \right) = \left[\begin{array}{cc} \boldsymbol{X}_{11} & \boldsymbol{X}_{12} \\ \boldsymbol{0} & \boldsymbol{X}_{22} \end{array} \right] = \left[\begin{array}{cc} \boldsymbol{X}_{11} & \boldsymbol{\Phi}_k^{-1} \tilde{\boldsymbol{Q}}_k \\ \boldsymbol{0} & \boldsymbol{\Phi}_k^\intercal \end{array} \right] \tag{8}$$

which leads to the result $\boldsymbol{\Phi}_k = \boldsymbol{X}_{22}^\intercal$ and $\tilde{\boldsymbol{Q}}_k = \boldsymbol{\Phi}_k \boldsymbol{X}_{12}$. Assuming a reasonably fast integration step, these quantities can be approximated by $\boldsymbol{\Phi}_k \approx \boldsymbol{I} + \boldsymbol{F}_k \Delta t$ and $\tilde{\boldsymbol{Q}}_k \approx \boldsymbol{Q}_k \Delta t$.

C. High-Fidelity Atmosphere Models

High-fidelity atmosphere models can also be incorporated into the state estimate as prior information. These atmosphere models are assumed to be computationally intensive enough such that implementation within the algorithm is infeasible. Instead, the high-fidelity atmosphere model data can be incorporated using table look-ups where the atmospheric conditions and uncertainties are tabulated as a function of altitude along some nominal trajectory. The model of this form produces an estimate of the atmospheric conditions $\boldsymbol{x}_k$, along with an associated error covariance matrix $\boldsymbol{T}_k$.

D. Data Fusion Algorithm

The atmospheric state estimate can be determined from a fusion of the available data sources, including the FADS pressure measurements, and information from the low and high fidelity models. The algorithm is in the form of a nonlinear weighted least-squares solution with the model data incorporated as prior estimates.

The pressure measurement model can be approximated by means of the truncated series expansion

$$\boldsymbol{p}_k \approx \boldsymbol{h}(\bar{\boldsymbol{x}}_k, \boldsymbol{u}_k) + \boldsymbol{H}_k (\boldsymbol{x}_k - \bar{\boldsymbol{x}}_k) + \tilde{\boldsymbol{\epsilon}}_k \tag{9}$$

where $\bar{\boldsymbol{x}}_k$ is some reference state, $\boldsymbol{H}_k$ is the measurement sensitivity matrix, and $\tilde{\boldsymbol{\epsilon}}_k$ is an error state that include pressure measurement and model uncertainties in addition to uncertainties in the navigation state $\boldsymbol{u}_k$. The covariance of $\tilde{\boldsymbol{\epsilon}}_k$ is given by $\tilde{\boldsymbol{R}}_k = \boldsymbol{R}_k + \boldsymbol{J}_k \boldsymbol{\Omega}_k \boldsymbol{J}_k^\intercal$.

The atmospheric state estimation problem can be reduced to a linear regression problem of the form $\boldsymbol{y}_k = \boldsymbol{H}_k \boldsymbol{x}_k + \boldsymbol{\epsilon}_k$, where $\boldsymbol{y}_k = \boldsymbol{p}_k - \boldsymbol{h}(\bar{\boldsymbol{x}}_k, \boldsymbol{u}_k) + \boldsymbol{H}_k \bar{\boldsymbol{x}}_k$. By virtue of the Gauss–Markov theorem, the best linear unbiased

estimate of $\boldsymbol{x}_k$ is the weighted least-squares solution,[16] where the atmospheric model data are treated as prior observations

$$\hat{\boldsymbol{x}}_k = \left(\boldsymbol{H}_k^\intercal \tilde{\boldsymbol{R}}_k^{-1} \boldsymbol{H}_k + \boldsymbol{S}_k^{-1} + \boldsymbol{T}_k^{-1}\right)^{-1} \left(\boldsymbol{H}_k^\intercal \tilde{\boldsymbol{R}}_k^{-1} \boldsymbol{y}_k + \boldsymbol{S}_k^{-1} \bar{\boldsymbol{x}}_k + \boldsymbol{T}_k^{-1} \boldsymbol{x}_h\right) \tag{10}$$

Since the relationship between the states and the measurement is nonlinear, the estimation scheme can be iterated until convergence by successively replacing $\bar{\boldsymbol{x}}_k$ by $\hat{\boldsymbol{x}}_k$. Then, the state estimate error covariance matrix $\hat{\boldsymbol{P}}_k$ can then be computed from

$$\hat{\boldsymbol{P}}_k = \left(\boldsymbol{H}_k^\intercal \tilde{\boldsymbol{R}}_k^{-1} \boldsymbol{H}_k + \boldsymbol{S}_k^{-1} + \boldsymbol{T}_k^{-1}\right)^{-1} \tag{11}$$

After incorporating the pressure measurement data and prior information from the atmospheric models, the best estimate of the atmospheric state and its covariance can be propagated forward in time to the next measurement sample using the low-fidelity model equations of motions given in Eqs. (6) and (7). Note that this framework is essentially an iterative extended Kalman filter, with the additional incorporation of prior data from the high-fidelity model tables. In a sense, the proposed technique is an optimal blending of FADS pressure measurements and a virtual air data system[19] that uses only forecast atmosphere data.

E. Backward Smoothing

The estimate of the atmospheric state at the end of the process has incorporated all available data and thus represents the best possible estimate of the atmosphere. In a post-flight processing scenario, this best estimate can be smoothed backwards to the initial time in order to map this information over the entire trajectory. This process is known as fixed-interval smoothing. One well known solution of the fixed interval smoothing problem is the Rauch-Tung-Striebel smoother.[18] The backward recursion formulas are given by

$$\boldsymbol{C}_k = \hat{\boldsymbol{P}}_{k|k} \boldsymbol{\Phi}_k^\intercal \hat{\boldsymbol{P}}_{k+1|k}^{-1} \tag{12}$$

$$\hat{\boldsymbol{x}}_{k|N} = \hat{\boldsymbol{x}}_{k|k} + \boldsymbol{C}_k \left[\hat{\boldsymbol{x}}_{k+1|N} - \hat{\boldsymbol{x}}_{k|k} - \boldsymbol{f}\left(\hat{\boldsymbol{x}}_{k|k}, \boldsymbol{u}_k\right) \Delta t\right] \tag{13}$$

$$\hat{\boldsymbol{P}}_{k|N} = \hat{\boldsymbol{P}}_{k|k} + \boldsymbol{C}_k \left[\hat{\boldsymbol{P}}_{k+1|N} - \hat{\boldsymbol{P}}_{k+1|k}\right] \boldsymbol{C}_k^\intercal \tag{14}$$

The backward smoothing procedure begins with the final state estimate given all available measurements, $\hat{\boldsymbol{x}}_{N|N}$ and its covariance, $\hat{\boldsymbol{P}}_{N|N}$ and propagates from $k = N$ backward to $k = 1$ using the relations given above.

F. Aerodynamic State Transformations

The atmospheric state (winds, pressure, and density) are outputs of the proposed FADS data processing algorithm (from either the forward filter for possible real-time applications, or the backward smoother for post-flight processing). The atmospheric state can readily be combined with the INS state solution (velocity and attitude) to produce estimates of aerodynamic states, including angle of attack, sideslip, Mach number, dynamic pressure, and vehicle aerodynamic coefficients. Uncertainties can be mapped from the atmospheric and INS states into the aerodynamic states through linear covariance analysis. The equations of the transformation from atmospheric and INS states to aerodynamic states are readily available in various sources such as Ref. 20 and are not repeated here.

III. Application to Mars Science Laboratory

On August 5th 2012, the Mars Science Laboratory (MSL) entry vehicle successfully entered the Mars atmosphere and landed the Curiosity rover safely on the surface of the planet in Gale crater. The Mars Science Laboratory entry vehicle was comprised of a 70-degree sphere-cone heatshield and backshell consisting of a stack of three truncated cones. The forebody was similar to the heatshield geometry developed for the Viking Mars landers. Phenolic Impregnated Carbon Ablator (PICA) was used for the thermal protection system material. The backshell configuration was also similar to Viking, with a third cone section added to accommodate the parachute volume. The MSL vehicle as-built outer mold line is shown in Fig. 1(a). During most of entry, the capsule used a radial center of mass offset to fly at an angle of attack (approximately 16 degrees at hypersonic conditions). This attitude produced lift to fly a guided entry profile, reducing the landing footprint to a much smaller size than any previous Mars mission. To fly the guided entry, the vehicle carried four pairs of Reaction Control System (RCS) jets to perform maneuvers and damp rates. The four pairs of jets could be fired rapidly in different combinations to provide control torques about roll, pitch, yaw, or any other axis by modulating the pulses of the jet.

MSL carried with it an instrumentation package designed to measure the aerodynamic and aerothermal environments during atmospheric entry. This instrumentation package was known as the MSL Entry, Descent, and Landing

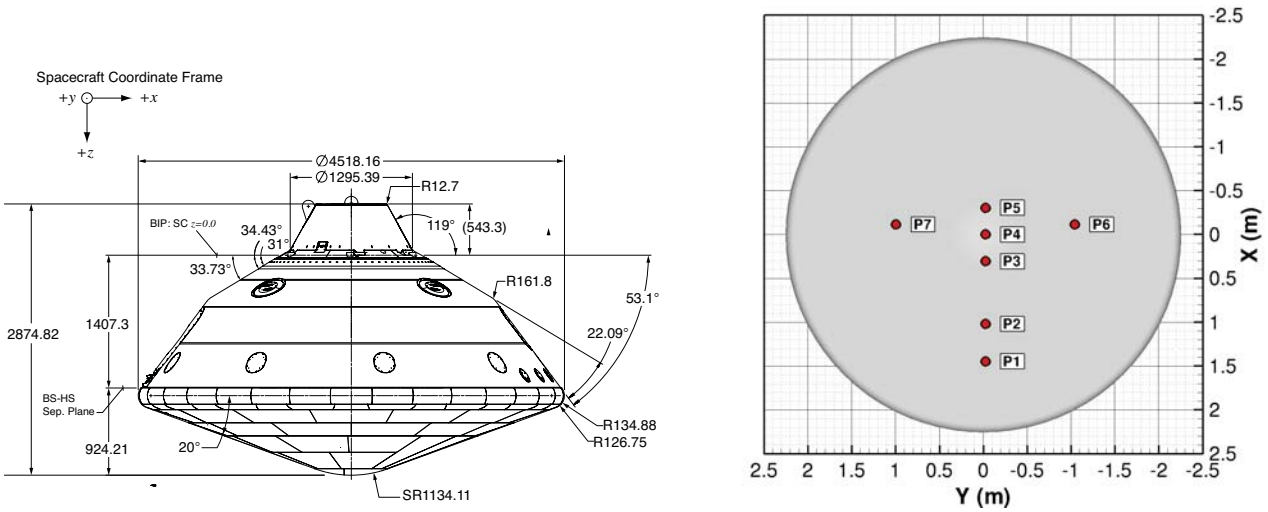

(a) As Built MSL Outer Mold Line

(b) MEDLI/MEADS Geometry (Looking Aft)

Figure 1: Vehicle Geometry

Instrumentation (MEDLI),[21] which consists of three major subsystems: the Mars Entry Atmospheric Data System (MEADS), the MEDLI Integrated Sensor Plugs (MISP), and the Sensor Support Electronics (SSE). The MEADS consisted of seven pressure transducers connected to flush orifices in the heat shield to measure pressures across the vehicle forebody. The MISP devices were a system of seven thermocouple and recession sensors that provided aerothermal measurements of the heat shield performance. The SSE provided power to the sensors, conditioned their signals, and transmitted the data to storage on the Curiosity rover. The MEDLI sensors provided measurements that were used for trajectory reconstruction and engineering validation of aerodynamic, atmospheric, and thermal protection system models in addition to Earth-based systems testing procedures. The MEDLI data and its usage for reconstructing the aerodynamic and aerothermal performance of the MSL entry vehicle are described in Refs. 14 and 22–26.

A. Flight Reconstruction

This section describes the results of applying the new full state INS-aiding approach to the MEADS atmospheric reconstruction. The high-fidelity atmosphere models are based on combined mesoscale models, which include the Mars Mesoscale Model v5 (MMM5)[27] and the Mars Regional Atmosphere Model System (MRAMS).[28] The mesoscale atmosphere models provided estimates of the mean and variability of atmospheric values from the surface to approximately 50 km altitude. Further details of how the models were utilized for MSL can be found in Ref. 29. Uncertainties in the INS solution are based on linear covariance propagation of the MSL navigation filter algorithm.[30]

Figures 2–4 shows a comparison of the basic (unaided) FADS algorithm and the velocity-based INS-Aided FADS algorithm from Ref. 14. Both algorithms produce good estimates of dynamic pressure, but due to the inherent weak observability of static pressure from surface pressure measurements alone,[14] the unaided FADS algorithm produces wildly varying estimates of Mach number. As a consequence, there is some angle of attack error buildup in the unaided FADS algorithm since the algorithm assumes an erroneous Mach number, and thus looks up pressures in the CFD database at an incorrect flight condition. The velocity-based INS-aiding algorithm stabilizes the estimates of Mach number and static pressure. The new proposed tightly-coupled INS/FADS algorithm produces estimates that are similar to the velocity-based INS aiding algorithm.

Fig. 4 shows a comparison of the density and static pressure estimates from the three algorithms. While the density estimates are comparable between the three algorithms, the static pressure estimate from the unaided FADS algorithm is highly erratic and completely unreasonable due to the inherent weak observability of this method. Both the aiding algorithms produce reasonable estimates of static pressure. Some slight differences are apparent between the two aiding algorithms in the estimate of atmospheric density. Here, differences arise due to the treatment of winds in the two algorithms. The velocity-aiding algorithm assumes zero winds, and computes density directly from dynamic pressure and INS relative velocity. Thus, non-zero winds are a possible error source in the algorithm which would produce a biased result. The tightly-coupled algorithm produces a slightly different estimate due to the fact that winds are estimated from the pressure measurements and thus the estimated density is unbiased in the presence

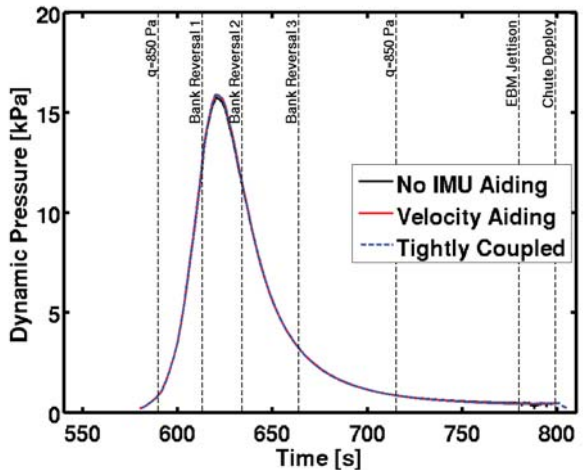

(a) Dynamic Pressure

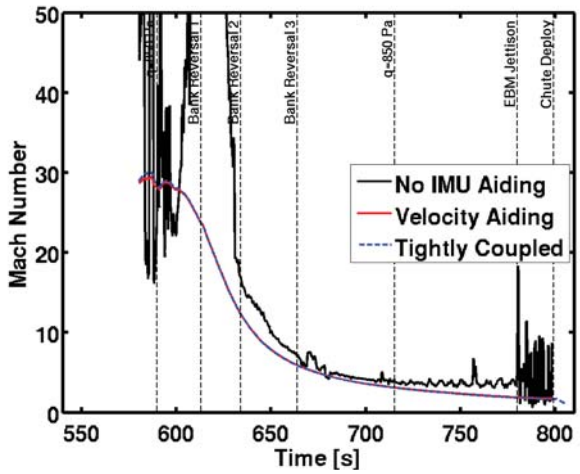

(b) Mach Number

Figure 2: Dynamic Pressure and Mach Number

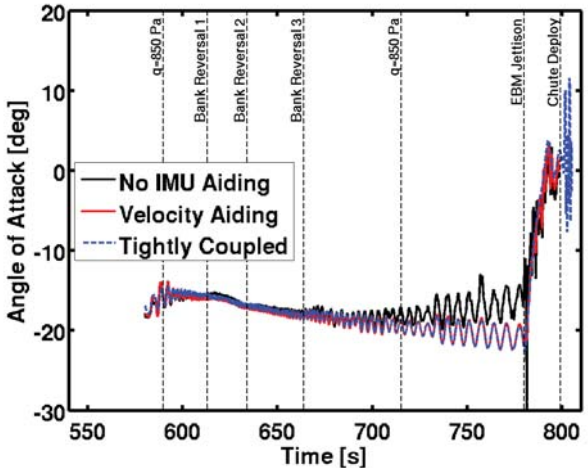

(a) Angle of Attack

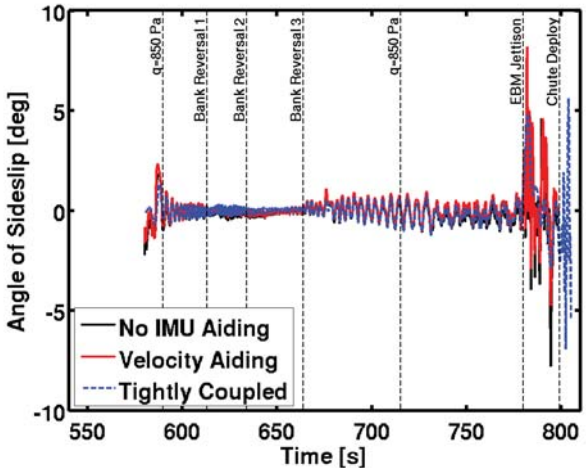

(b) Angle of Sideslip

Figure 3: Aerodynamic Angles

of winds. The difference between these density profiles is consistent with a tailwind, which would have the effect of reducing the apparent density if winds are otherwise assumed to be zero.

The reconstructed atmospheric winds are shown in Fig. 5. These figures show comparisons between the winds derived from the velocity aiding solution and the new tightly-coupled INS/FADS algorithm. Recall that the winds computed from the velocity-aided solution were obtained by the method proposed in Ref. 2 wherein the wind estimates are produced by reconciling differences between FADS (wind-relative) and INS (planet-relative) angles of attack and sideslip. This algorithm produces wind estimate results that vary wildly over the trajectory, and for the most part produces unreasonable results. The algorithm is better behaved at lower Mach numbers where winds are more observable because they are a larger portion of the total air-relative velocity.

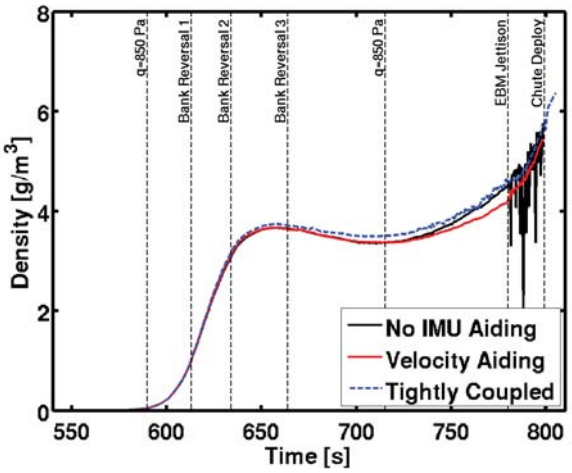

(a) Density

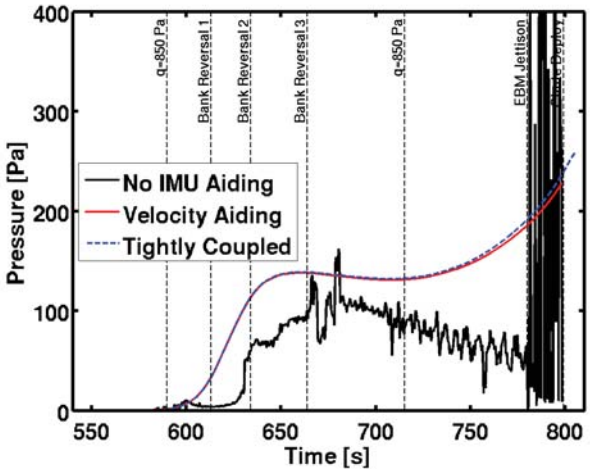

(b) Pressure

Figure 4: Atmosphere

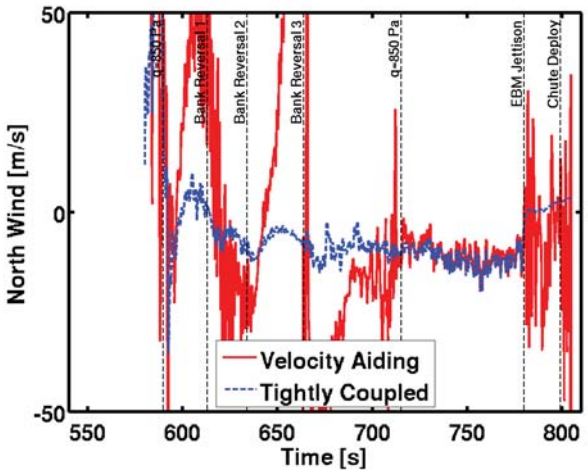

(a) North Wind

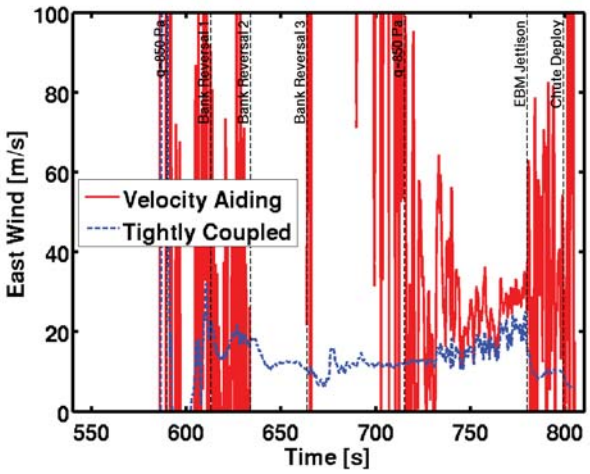

(b) East Wind

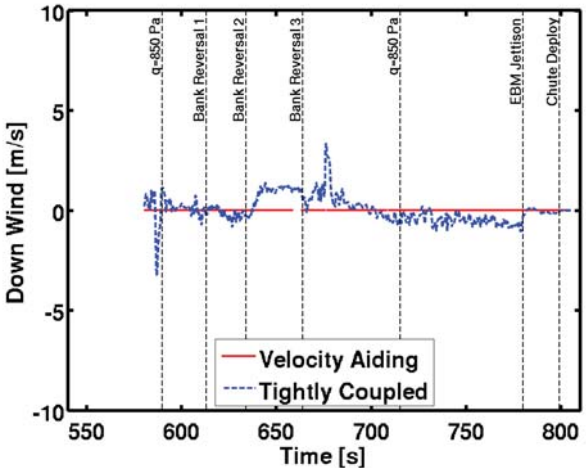

(c) Down Wind

Figure 5: Winds

The new tightly-coupled INS/FADS algorithm produces reasonable wind estimates over the entire entry trajectory. These wind estimates indicate a north wind component of approximately -10 m/s and an east wind component of approximately 20 m/s over much of the entry trajectory. For the MSL entry trajectory, the north and east winds are essentially pure cross and tail winds, respectively. These estimates are reasonable given the atmospheric uncertainties,[24] and moreover support circumstantial evidence for winds based on the vehicle entry guidance response[31] and trajectory.[32] The wind estimates are also consistent with post-flight full state Kalman filter/smoother results from Ref. 14. Note that following the Entry Balance Mass (EBM) jettison event, the pressure data becomes corrupted by structural vibrations due to pyrotechnic shocks. These shocks cause the transducer diaphragms to vibrate, which increases the noise in the pressure data. This increased noise level shifts the filter weighting such that the wind estimates revert to the tabulated atmosphere model following the EBM Jettison event.

B. Observability Analysis

The MSL entry vehicle flew a guided entry, using bank reversals to control downrange position during hypersonic flight.[31] A time history of the bank profile and resulting vehicle yaw attitude is shown in Fig. 6(a). These bank reversals are designed for the purpose of EDL guidance, but they have the secondary benefit of increasing the observability of winds along the trajectory. The observability of the wind states along the trajectory can be assessed via the discrete-time observability Gramian, defined as[16]

$$\boldsymbol{W}_o = \sum_{k=0}^{N} \boldsymbol{\Phi}_k^{\mathsf{T}} \boldsymbol{H}_k^{\mathsf{T}} \boldsymbol{H}_k \boldsymbol{\Phi}_k \tag{15}$$

One scalar measure of the observability of the system is the minimum singular value of the observability Gramian.[33] If the minimum singular value is small, the system difficult to observe. Likewise, large values of the minimum singular value indicate the opposite. Other observability metrics include the rank, determinant, eigenvalues, maximum singular value, trace, and condition number of the observability Gramian.[33] The minimum singular value of the observability Gramian, σ_{min}, and its time rate of change along the MSL entry trajectory are shown in Fig. 6(b). By examining the rate of change of σ_{min}, it is apparent that the minimum singular value starts to increase just after the time of the bank reversals. The implication is that the bank reversals have the effect of adding information content to the system.

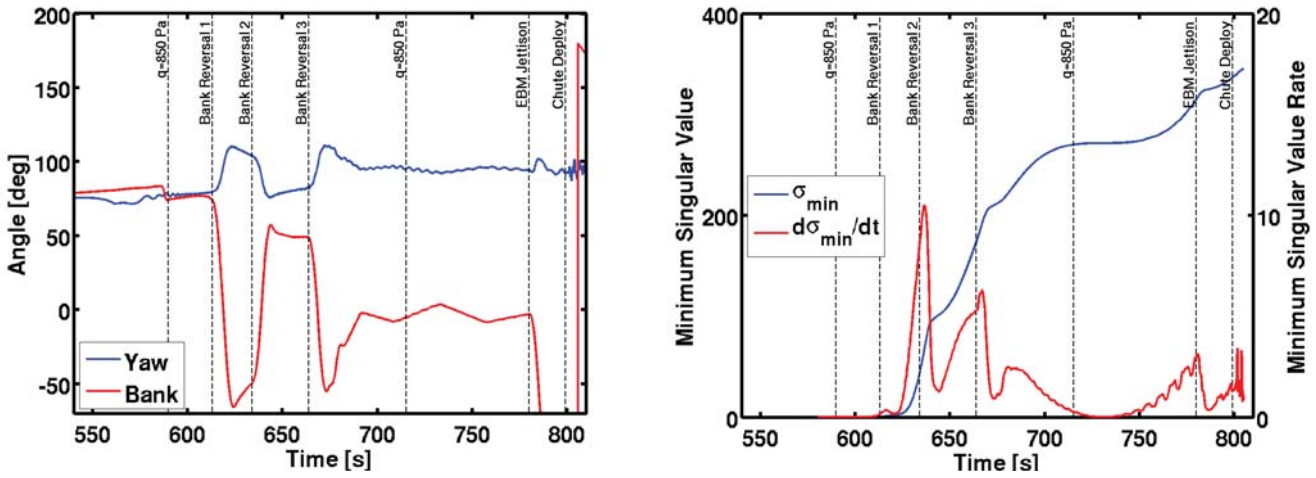

(a) Bank and Yaw Angles

(b) Observability Index

Figure 6: Bank Profile and Observability

The source of the information content can be gleaned by examining the pressure measurement sensitivities with respect to the states along the trajectory. Fig. 7 shows the pressure measurement sensitivity with respect to density and static pressure. These plots show that the pressure measurements are highly sensitive to density, which is to be expected. The sensitivity with respect to density does not show any correlation to bank maneuvers. The static pressure sensitivity shows some correlation to the bank profile.

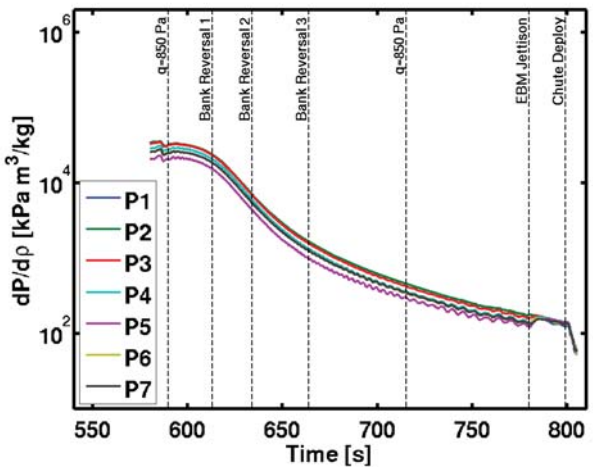

(a) Sensitivity to Density

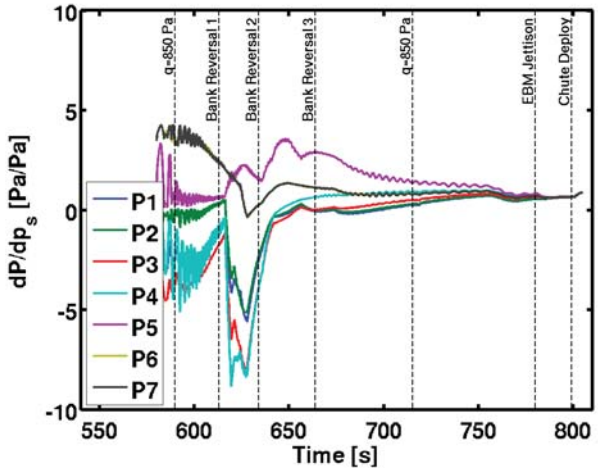

(b) Sensitivity to Pressure

Figure 7: Pressure Measurement Sensitivities to Atmosphere States

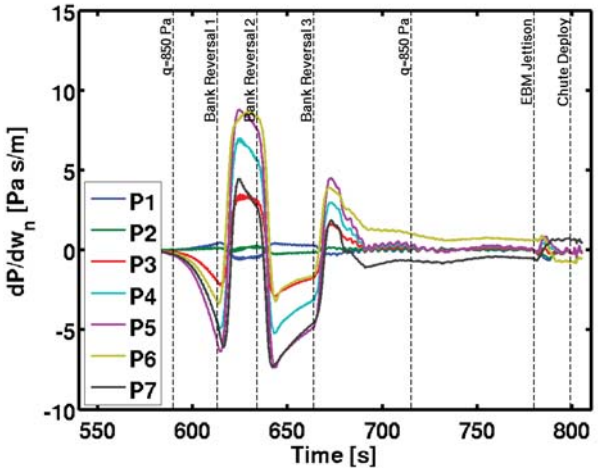

(a) Sensitivity to North Wind

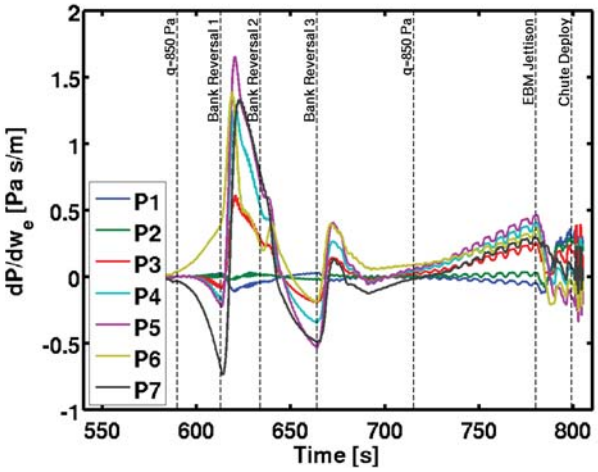

(b) Sensitivity to East Wind

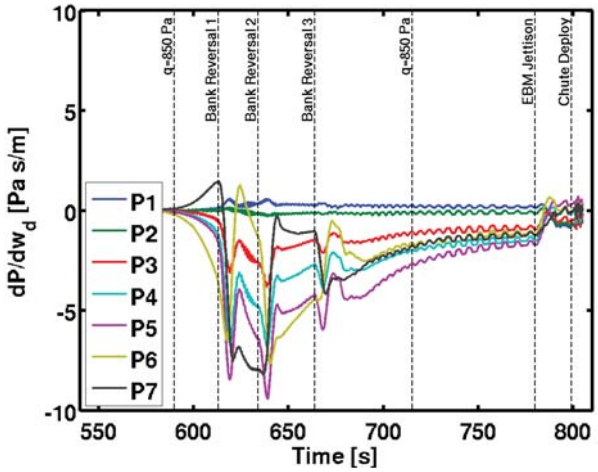

(c) Sensitivity to Down Wind

Figure 8: Pressure Measurement Sensitivities to Wind States

The pressure measurement sensitivities with respect to the wind components are shown in Fig. 8. These sensitivities show a strong correlation to the bank profile. The implication is that the bank maneuvers add information content about the wind profile. It can also be seen that the pressures are more sensitive to the northerly component of the wind. As stated in the previous section, the northerly wind corresponds to a crosswind for the MSL entry trajectory. A crosswind corresponds to a non-zero inertial sideslip angle such that winds can be determined easily from the sideslip pressure port measurements. Head/tail winds are more difficult for the filter to resolve because the centerline ports are strong functions of both the angle of attack and dynamic pressure, which serves to couple the head/tail wind with density as well as the downward wind component.

The observability of winds due to the bank reversals has several consequences. Firstly, a purely ballistic entry with no guidance may not be able to resolve winds along the trajectory. Secondly, the sensitivity of winds to bank reversals opens up the possibility of designing maneuvers to maximize the observability of winds along the trajectory. Observability-based trajectory optimization for flowfield estimation has been proposed in Ref. 34, for example. Such a process would be akin to designing system identification maneuvers for estimating aircraft aerodynamic parameters.

IV. Implications for the Mars 2020 Mission

Another MEDLI-like system of instruments is planned to be flown on the Mars 2020 mission. This instrumentation system, known as MEDLI2,[35] will acquire FADS pressure data to be used for the reconstruction of atmospheric states and vehicle aerodynamics during entry. The focus of the pressure system on MEDLI2 is geared toward estimating aerodynamics in the supersonic regime of flight, where some questions remain regarding the aerodynamic reconstruction of MSL.[25] To this end, the forebody pressure system will carry one transducer with a full scale range of 5 psi (the same as MSL transducers) to measure stagnation pressure over the entire entry trajectory (which in turn yields estimates of dynamic pressure and density), and six transducers with a full scale range of 1 psi to more accurately measure the atmosphere and aerodynamics in the supersonic regime of flight (roughly Mach 6 and below). In addition, one transducer will be installed on the backshell to measure the base pressure and its contribution to drag. Since the focus of this instrumentation is on supersonic measurements, estimates of winds are far more critical to interpreting the reconstructed aerodynamics. Thus, the algorithm described in this paper is expected to prove useful in the post-flight data reconstruction effort.

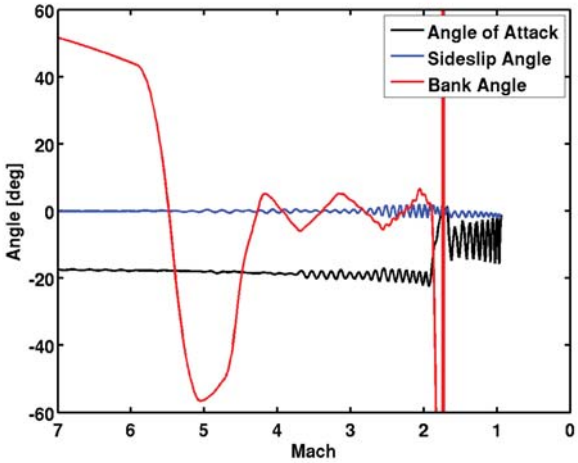

Figure 9: Reference Trajectory

The following two sections describe the design of the pressure port layout to optimize atmospheric state observability, and linear covariance analysis of the estimator performance for a given pressure measurement uncertainty. The reference trajectory on which these analyses are based in shown in Fig. 9.

A. Port Placement Optimization

The reformulated wind estimation algorithm described in this paper enables a straightforward method to optimize the FADS port layout in order to provide the best state estimates for a given trajectory. The optimization can be achieved by solving for pressure port locations that maximize the observability (or, equivalently, minimize the unobservability) of the atmospheric state based on the observability Gramian. Sensor placement optimization for

observability was first suggested in Ref. 36, and has subsequently been studied for a wide range of applications such as structural vibration,[37] chemical reactors,[38] airfoil wake estimation,[39] and Mars entry navigation.[40]

Another approach, suggested in Ref. 41, involves sensor placement optimization that minimizes the trace of a weighted state covariance matrix. This approach has been utilized in the past for FADS pressure port location optimization in Refs. 42–44 (minimum RMS errors were utilized in Ref. 42). This approach has the drawback that the optimal sensor locations become dependent on modeling assumptions such as the process and measurement noise covariance and the choice of the weighting matrix.

In this paper, the pressure port locations are chosen to directly maximize the observability of the system by minimizing the reciprocal of the minimum singular value of the observability Gramian. In this method, the optimal port locations are functions only of the reference trajectory and the CFD pressure distribution model. A sequential quadratic programming method is used to solve the optimization problem. Several constraints are imposed on the optimization, namely that the ports are constrained to lie within a boundary in order to not be placed too near the shoulder and away from leeside turbulent conditions. Ports 1, 2, and 5 are constrained to lie at the stagnation regions before and after the entry ballast mass ejections, which occurs shortly before parachute deployment and involves a change to the trim angle of attack. In addition, the remaining ports (3/4 and 6/7) are constrained to be in symmetric pairs across the vehicle pitch plane of symmetry.

A candidate port arrangement is shown in Figure 10(a). The dashed curves represent the boundary of admissible port locations. Note that the red square location indicates a hypersonic pressure port with full scale range of 5 psi, and the blue circle markers represent supersonic ports with full scale range of 1 psi. The Port pressures along the trajectory in the supersonic regime are shown in Figure 10(b). Note that the supersonic pressure measurements are saturated above 1 psi.

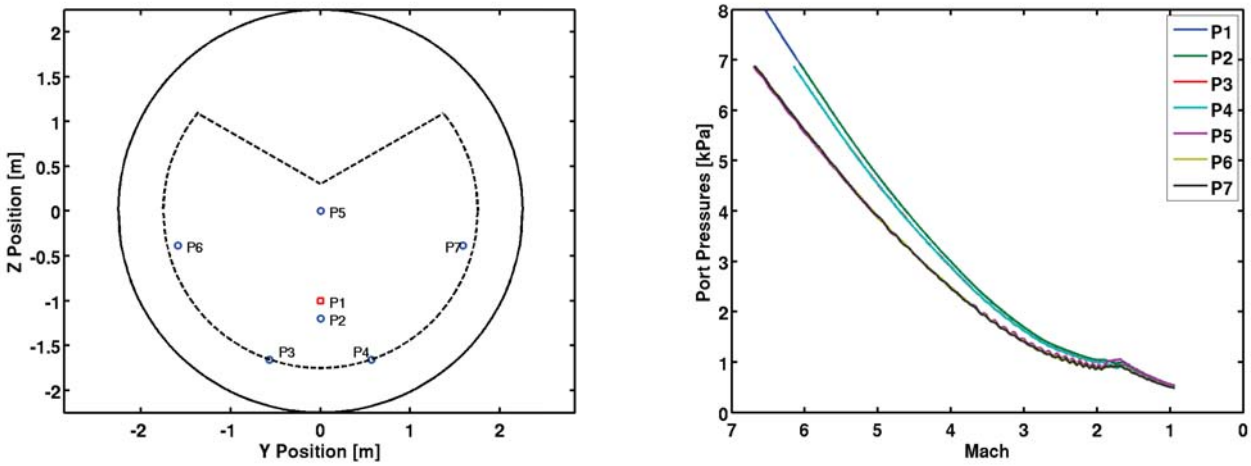

(a) Candidate Port Arrangement

(b) Pressures Along Trajectory

Figure 10: Port Arrangement

Pressure measurement sensitivities with respect to the dynamic pressure, density, and aerodynamic flow angles are shown in Fig. 11. These results indicate that ports 1 and 2 provide the most information about the freestream dynamic pressure, followed closely by ports 3 and 4. This result is expected since these ports lie within or closely bound the stagnation region on the forebody. The same trend is evident in the pressure measurement sensitivity to freestream density. Conversely, ports 5, 6, and 7 provide the most information about the angle of attack. The angle of sideslip is primarily sensitive to ports 6/7 and 3/4 which is also expected since these ports lie in symmetric pairs off the vehicle pitch plane of symmetry.

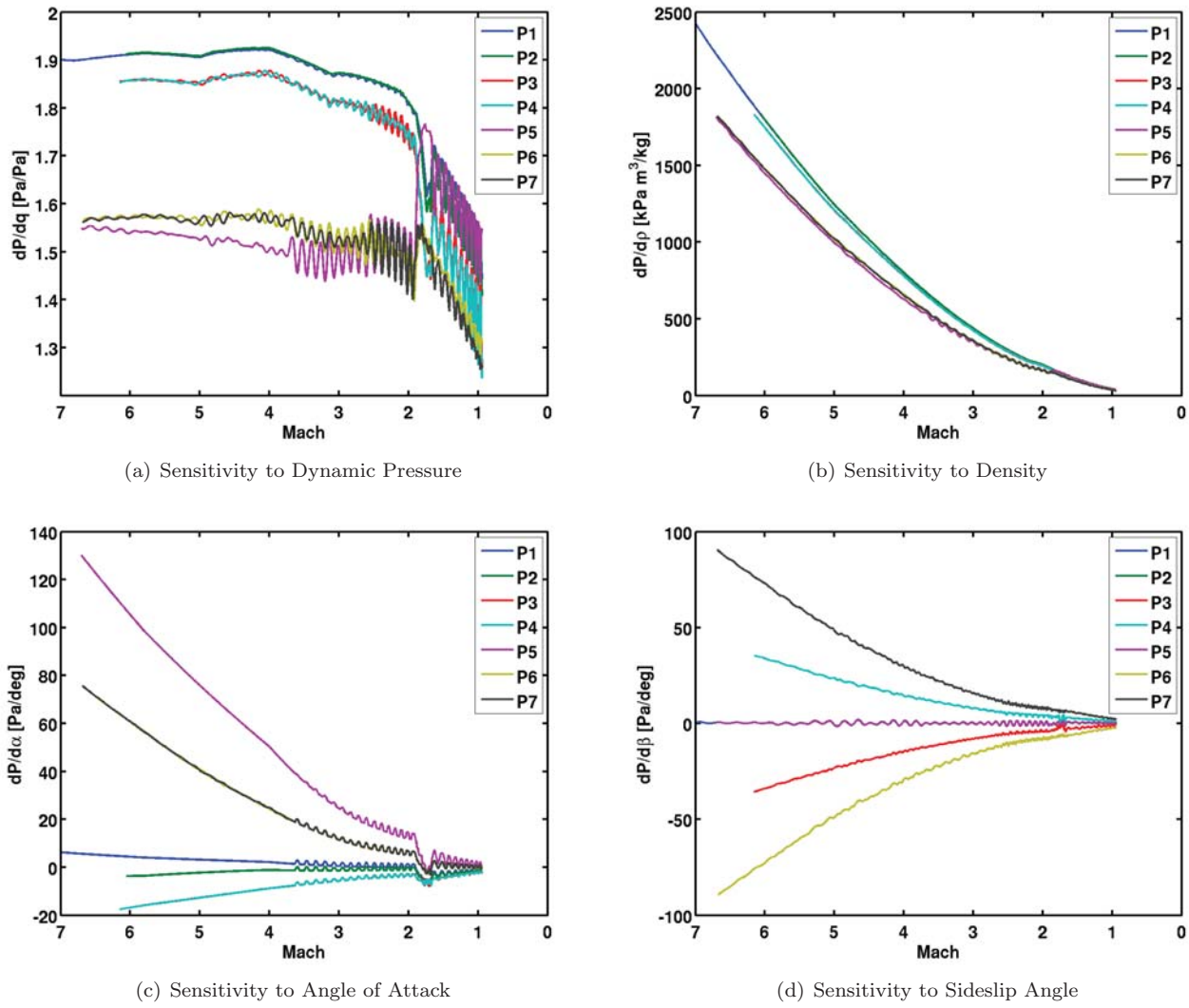

(a) Sensitivity to Dynamic Pressure

(b) Sensitivity to Density

(c) Sensitivity to Angle of Attack

(d) Sensitivity to Sideslip Angle

Figure 11: Pressure Measurement Sensitivities to Dynamic Pressure, Density, and Flow Angles

Pressure measurement sensitivities to the wind states are shown in Fig. 12. These results show that the north wind component (effectively a cross wind for this trajectory) is mainly sensitive to ports 3/4 and 6/7. This sensitivity is in keeping with the sideslip sensitivity to cross wind described in Section III.B. Likewise, east and down wind port sensitivities follow the angle of attack sensitivities. Additionally, note that the pressure measurements are more sensitive to cross winds than to head winds.

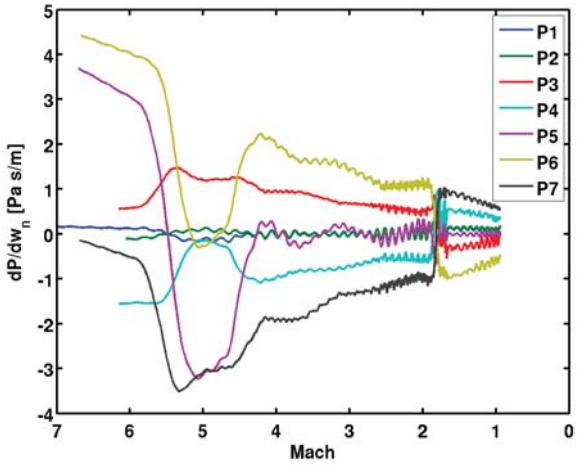

(a) Sensitivity to North Wind

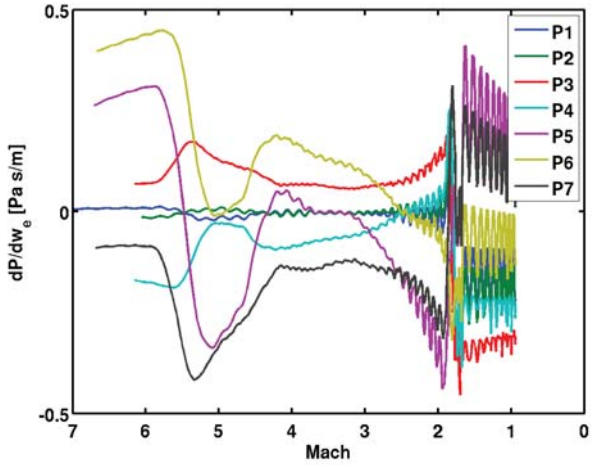

(b) Sensitivity to East Wind

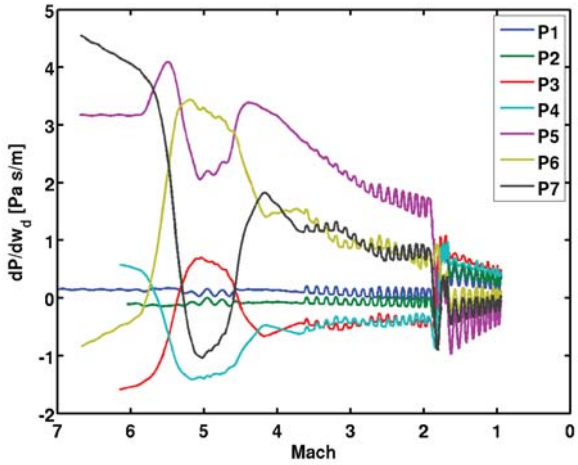

(c) Sensitivity to Down Wind

Figure 12: Pressure Measurement Sensitivities to Wind States

B. Linear Covariance Analysis

This section describes a linear covariance analysis of the estimator performance. The uncertainties are propagated along a nominal trajectory, assuming pressure measurement accuracies of 0.1% of full scale, and pressure port locations shown in Figure 10(a). CFD uncertainties and INS uncertainties are ignored for this analysis, simply to show a comparison between the velocity-aided and tightly-coupled algorithms for a given pressure measurement uncertainty.

Fig. 13 shows the linear covariance analysis results for estimates of dynamic pressure and Mach number. The results indicate that the dynamic pressure estimates corresponding to the new tightly-coupled algorithm are roughly the same precision as the velocity-aided algorithm at high Mach numbers, and the new algorithm becomes more precise than the velocity-aided algorithm as the Mach number decreases. The Mach number reconstruction corresponding to the tightly-coupled algorithm is superior to the velocity-aided algorithm across the range of Mach numbers. This result is due to both an enhanced estimate of the speed of sound as well as improved estimate of winds (which in turn produces an improved estimate of wind-relative velocity), which is shown in the following figures.

A comparison of results for the aerodynamic flow angles is shown in Fig. 14. The results are fairly comparable, although the tightly-coupled algorithm produces a slightly improved result over that of the velocity-aided algorithm. This improvement is due to the incorporation of additional information in the form of the INS attitude estimates.

Uncertainty analysis results for the atmosphere states are shown in Fig. 15. These results indicate that the tightly-coupled algorithm is able to produce improved estimates of the atmospheric states. The density estimate is improved

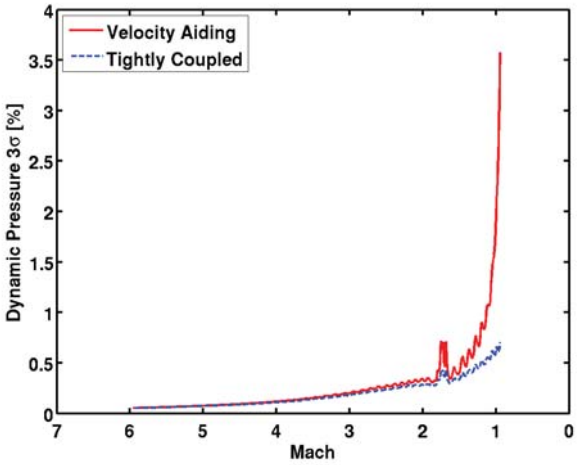

(a) Dynamic Pressure

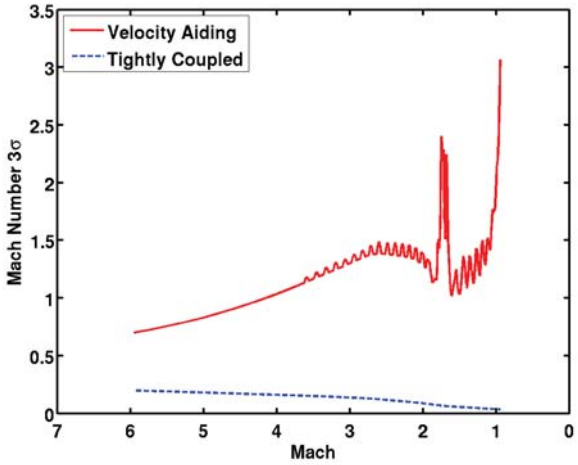

(b) Mach Number

Figure 13: Linear Covariance Analysis Results: Dynamic Pressure and Mach Number

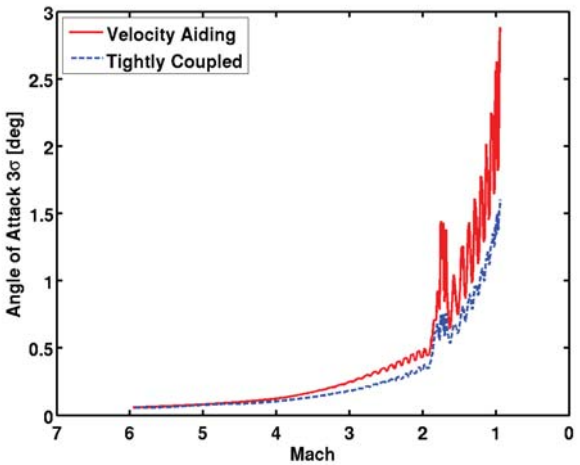

(a) Angle of Attack

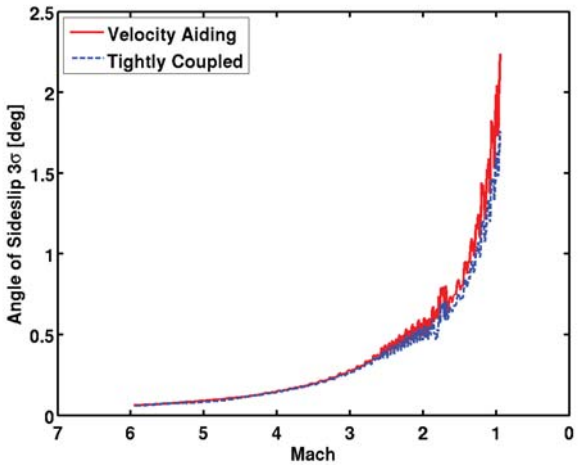

(b) Angle of Sideslip

Figure 14: Linear Covariance Analysis Results: Aerodynamic Flow Angles

because of improved estimates of the wind state. The velocity-aided pressure reconstruction uncertainty is a highly conservative estimate of the true uncertainty, because this pressure estimate arises by integrating the hydrostatic equation, treating each density sample as uncorrelated with previous estimates. In reality, these estimates are expected to have some level of correlation, which would have the effect of reducing the pressure estimate uncertainty.

Finally, wind estimate uncertainties are shown in Fig. 16. The tightly coupled algorithm produces improved estimates of winds by incorporating INS attitude measurements directly into the estimation process.

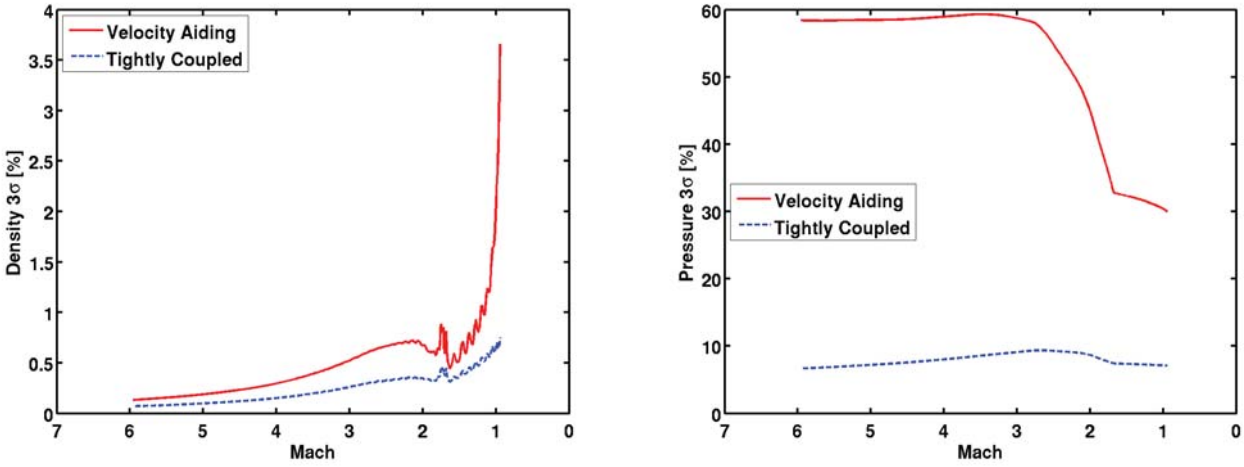

(a) Density (b) Pressure

Figure 15: Linear Covariance Analysis Results: Atmosphere

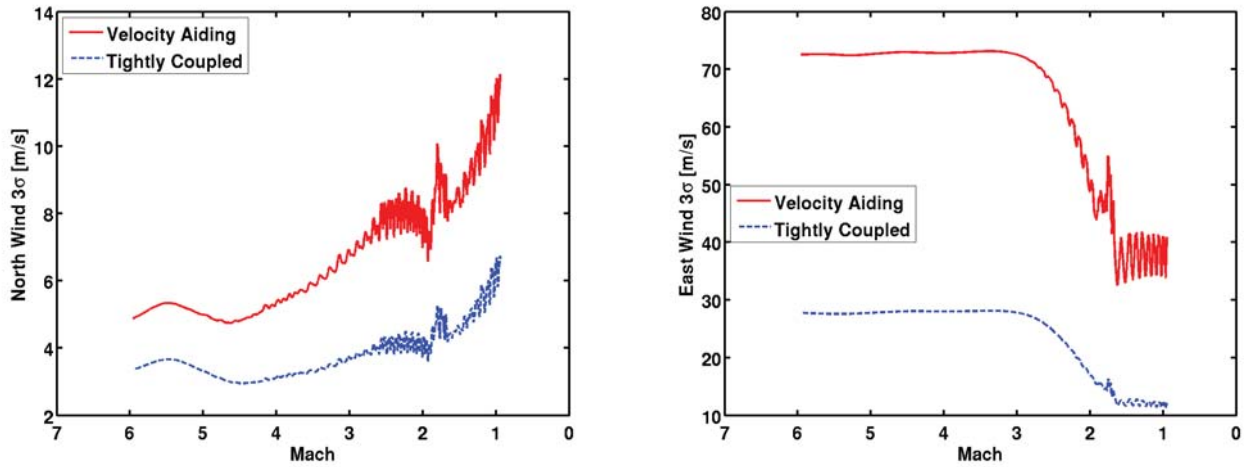

(a) North Wind (b) East Wind

Figure 16: Linear Covariance Analysis Results: Winds

V. Conclusions

A new inertial navigation system aiding approach is developed for flush air data sensing systems. The approach utilizes a full-state aiding (velocity and attitude) opposed to past approaches which use only velocity magnitude. The advantage of the new aiding approach is that winds can directly be estimated from the measured pressures, rather than being inferred from discrepancies between inertial angle of attack and wind-relative angle of attack that can sometimes lead to singularities or other issues with observability of winds. The algorithm produces a reasonable estimate of the atmospheric conditions based on flight data from the Mars Science Laboratory entry vehicle that was acquired in August 2012. In particular, the estimates of winds are consistent with circumstantial evidence based on vehicle dynamics and with full-order Kalman filter/smoother results. Linear covariance analysis results indicate that the new algorithm produces enhanced atmospheric state estimates when compared to the existing state-of-the-art air data processing algorithm. The algorithm is computationally straightforward such that real-time implementation is possible, although computational complexity/feasibility would need to be assessed for each particular application.

References

[1]Pruett, C. D., Wolf, H., Heck, M. L., and Siemers, P. M., "Innovative Air Data System for the Space Shuttle Orbiter," *Journal of Spacecraft and Rockets*, Vol. 20, No. 1, 1983, pp. 61–69.

[2]Kelly, G. M., Findlay, J. T., and Compton, H. R., "Shuttle Subsonic Horizontal Wind Estimation," *Journal of Spacecraft and Rockets,* Vol. 20, No. 4, 1983, pp. 390–397.

[3]Ellsworth, J. C. and Whitmore, S. A., "Simulation of a Flush Air–Data System for Transatmospheric Vehicles," *Journal of Spacecraft and Rockets*, Vol. 45, No. 4, 2008, pp. 716–732.

[4]Baumann, E., Pahle, J. W., Davis, M. C., and White, J. T., "X-43A Flush Airdata Sensing System Flight–Test Results," *Journal of Spacecraft and Rockets*, Vol. 47, No. 1, 2010, pp. 48–61.

[5]Kasich, D. and Cheng, P., "Flush Port / Inertially Blended Air Data Estimator," AIAA Paper 91-0670, January 1991.

[6]van den Kroonenberg, A., Martin, T., Buschman, M., Bange, J., and Vörsmann, P., "Measuring the Wind Vector Using the Autonomous Mini Aerial Vehicle M^2AV," *Journal of Atmospheric and Oceanic Technology*, Vol. 25, No. 11, 2008, pp. 1969–1982.

[7]Cho, A., Kim, J., Lee, S., and Kee, C., "Wind Estimation and Airspeed Calibration using a UAV with a Single-Antenna GPS Receiver and Pitot Tube," *IEEE Transactions on Aerospace and Electronic Systems*, Vol. 47, No. 1, 2011, pp. 109–117.

[8]Langelaan, J. W., Alley, N., and Neidhoefer, J., "Wind Field Estimation for Small Unmanned Aerial Vehicles," *Journal of Guidance, Control, and Dynamics*, Vol. 34, No. 4, 2011, pp. 1016–1030.

[9]Lee, J. H., Sevil, H. E., Dogan, A., and Hullender, D., "Estimation of Maneuvering Aircraft States and Time-Varying Wind with Turbulence," *Aerospace Science and Technology*, Vol. 31, 2013, pp. 87–98.

[10]Lie, F. and Gebre-Egziabher, D., "Synthetic Air Data System," *Journal of Aircraft*, Vol. 50, No. 4, 2013, pp. 1234–1249.

[11]Arain, B. and Kendoul, F., "Real-Time Wind Speed Estimation and Compensation for Improved Flight," *IEEE Transactions on Aerospace and Electronic Systems*, Vol. 50, No. 2, 2014, pp. 1599–1606.

[12]Karlgaard, C. D., Beck, R. E., O'Keefe, S. A., Siemers, P. M., White, B. A., Engelund, W. C., and Munk, M. M., "Mars Entry Atmospheric Data System Modeling and Algorithm Development," AIAA Paper 2009-3916, June 2009.

[13]Karlgaard, C. D., Beck, R. E., Derry, S. D., Brandon, J. M., Starr, B. R., Tartabini, P. V., and Olds, A. D., "Ares I-X Trajectory Reconstruction: Methodology and Results," *Journal of Spacecraft and Rockets*, Vol. 50, No. 3, 2013, pp. 641–661.

[14]Karlgaard, C. D., Kutty, P., Schoenenberger, M., Munk, M. M., Little, A., Kuhl, C. A., and Shidner, J., "Mars Science Laboratory Entry Atmospheric Data System Trajectory and Atmosphere Reconstruction," *Journal of Spacecraft and Rockets*, Vol. 51, No. 4, 2014, pp. 1029–1047.

[15]Cobleigh, B. R., Whitmore, S. A., Haering, E. A., Borrer, J., and Roback, V. E., "Flush Airdata Sensing (FADS) System Calibration Procedures and Results For Blunt Forebodies," AIAA Paper 99-4816, November 1999.

[16]Crassidis, J. L. and Junkins, J. L., *Optimal Estimation of Dynamic Systems, Second Edition*, Chapman & Hall, Boca Raton, FL, 2011.

[17]van Loan, C. F., "Computing Integrals Involving the Matrix Exponential," *IEEE Transactions on Automatic Control*, Vol. AC-23, No. 3, 1978, pp. 396–404.

[18]Rauch, H. E., Tung, F., and Striebel, C. T., "Maximum Likelihood Estimates of Linear Dynamic Systems," *AIAA Journal*, Vol. 3, No. 8, 1965, pp. 1445–1450.

[19]Nebula, F., Palumbo, R., Morani, G., and Corraro, F., "Virtual Air Data System Architecture for Space Reentry Applications," *Journal of Spacecraft and Rockets*, Vol. 46, No. 4, 2009, pp. 818–828.

[20]Ektin, B., *Dynamics of Atmospheric Flight*, John Wiley and Sons, Inc., New York, 1972.

[21]Munk, M. M., Little, A., Kuhl, C., Bose, D., and Santos, J., "The Mars Science Laboratory (MSL) Entry, Descent, and Landing Instrumentation (MEDLI) Hardware," AAS Paper 13-310, February 2013.

[22]Cheatwood, F. M., Bose, D., Karlgaard, C., Kuhl, C. A., Santos, J. A., and Wright, M. J., "Mars Science Laboratory (MSL) Entry, Descent, and Landing Instrumentation (MEDLI): Complete Flight Data Set," NASA TM-2014-218533, October 2014.

[23]Karlgaard, C. D., Van Norman, J., Siemers, P., Schoenenberger, M., and Munk, M., "Mars Entry Atmospheric Data System Modeling, Calibration, and Error Analysis," NASA TM-2014-218535, October 2014.

[24]Chen, A., Cianciolo, A., Vasavada, A., Karlgaard, C., Barnes, J., Cantor, B., Hinson, D., Kass, D., Lewis, S., Mischna, M., Rafkin, S., Tyler, D., "Reconstruction of Atmospheric Properties from the Mars Science Laboratory Entry, Descent, and Landing," *Journal of Spacecraft and Rockets*, Vol. 51, No. 4, 2014, pp. 1062–1075.

[25]Schoenenberger, M., Van Norman, J., Karlgaard, C. D., Kutty, P., and Way, D., "Assessment of the Reconstructed Aerodynamics of the Mars Science Laboratory Entry Vehicle," *Journal of Spacecraft and Rockets*, Vol. 51, No. 4, 2014, pp. 1076–1093.

[26]Bose, D., White, T., Mahzari, M., and Edquist, K., "Reconstruction of Aerothermal Environment and Heatshield Response of Mars Science Laboratory," *Journal of Spacecraft and Rockets*, Vol. 51, No. 4, 2014, pp. 1174–1184.

[27]Tyler, D., Barnes, J., and Skyllingstad, E., "Mesoscale and Large-Eddy Simulation Model Studies of the Martian Atmosphere in Support of Phoenix," *Journal of Geophysical Research*, Vol. 113, No. E3, 2008.

[28]Rafkin, S.C.R., Haberle, R., and Michaels, T., "The Mars Regional Atmospheric Modeling System (MRAMS): Model Description and Selected Simulations," *Icarus*, Vol. 151, pp. 228-256.

[29]Vasavada, A. R., Chen, A., Barnes, J. R., Burkhart, P. D., Cantor, B. A., Dwyer-Cianciolo, A. M., Fergason, R. L., Hinson, D. P., Justh, H. L., Kass, D. M., Lewis, S. R., Mischna, M. A., Murphy, J. R., Rafkin, S. C. R., Tyler, D., and Withers, P. G., "Assessment of Environments for Mars Science Laboratory Entry, Descent, and Surface Operations," *Space Science Reviews*, Vol. 170, 2012, pp. 793–835.

[30]Serricchio, F., San Martin, A. M., and Wong, E. C., "The MSL Navigation Filter," 10th Interplanetary Probe Workshop, San Jose, CA, June 2013.

[31]Mendeck, G. and McGrew, L., "Entry Guidance Design and Postflight Performance for 2011 Mars Science Laboratory Mission," *Journal of Spacecraft and Rockets*, Vol. 51, No. 4, 2014, pp. 1094–1105.

[32]Way, D., Davis, J., and Shidner, J., "Assessment of the Mars Science Laboratory Entry, Descent, and Landing Simulation," AAS Paper 13-420, February 2013.

[33]Krener, A. J. and Ide, K., "Measures of Unobservability," IEEE Conference on Decision and Control, 2009.

[34]DeVries, L., Majumdar, S. J., and Paley, D., "Observability-Based Optimization of Coordinated Sampling Trajectories for Recursive Estimation of a Strong, Spatially Varying Flowfield," *Journal of Intelligent and Robotic Systems*, Vol. 70, Nos. 1–4, 2013, pp. 527–544.

[35]Bose, D., White, T. R., Schoenenberger, M., Munk, M., Hwang, H. H., and Wright, H. S., "MSL Entry, Descent, and Landing Instrumentation: Return on Investment," 11th International Planetary Probe Workshop, Pasadena, CA, June 2014.

[36]Müller, P. C. and Weber, H. I., "Analysis and Optimization of Certain Qualities of Controllability and Observability for Linear Dynamical Systems," *Automatica*, Vol. 8, No. 3, 1972, pp. 237–246.

[37]Hac, A. and Liu, L., "Sensor and Actuator Location in Motion Control of Flexible Structures," *Journal of Sound and Vibration*, Vol. 167, No. 2, 1993, pp. 239–261.

[38]Waldraff, W., Dochain, D., Bourrel, S., and Magnus, A., "On the Use of Observability Measures for Sensor Location in Tubular Reactor," *Journal of Process Control*, Vol. 8, No. 5–6, 1998, pp. 497–505.

[39]Hinson, B. T. and Morgansen, K. A., "Observability-Based Optimal Sensor Placement for Flapping Airfoil Wake Estimation," *Journal of Guidance, Control, and Dynamics*, Vol. 37, No. 5, 2014, pp. 1477–1486.

[40]Yu, Z., Cui, P., and Zhu, S., "Observability-Based Beacon Configuration Optimization for Mars Entry Navigation," *Journal of Guidance, Control, and Dynamics*, 2014, to appear.

[41]Arbel, A., "Sensor Placement in Optimal Filtering and Smoothing Problems," *IEEE Transactions on Automatic Control*, Vol. 27, No. 1, 1982, pp. 94–98.

[42]Deshpande, S. M., Kumar, R. R., Seywald, H., and Siemers, P. M., "Air Data System Optimization Using a Genetic Algorithm," AIAA Paper 92-4466, 1992.

[43]Dutta, S., Braun, R., and Karlgaard, C. D., "Atmospheric Data System Sensor Placement Optimization for Mars Entry, Descent, and Landing," *Journal of Spacecraft and Rockets*, Vol. 51, No. 1, 2014, pp. 163–174.

[44]Dutta, S. and Braun, R., "Cramér-Rao Lower-Bound Optimization of Flush Atmospheric Data System Sensor Placement," *Journal of Spacecraft and Rockets*, to appear.